Desalination and Water Treatment
www.deswater.com

doi: 10.5004/dwt.2022.27963

245 (2022) 297–305
January

Synthesis of Sr@TiO_2 nanomaterials rapidly by microwave induced combustion method and measure its photocatalytic degradation properties of methyl orange wastewater

Yanqin Xu†, Hong Wu†, Zuntao Lv, Yuan Cao*

College of Chemistry and Chemical Engineering, Chongqing University, Chongqing 401331, China, Tel. +86 15923344273; emails: caoyuan@cqu.edu.cn (Y. Cao), xuyanqin666@163.com (Y. Xu), 202018131170@ cqu.edu.cn (H. Wu)

Received 27 July 2021; Accepted 4 November 2021

ABSTRACT

Sr-doped titania nanomaterials were prepared rapidly by microwave-induced combustion in 20 min, the oxidant and titanium were obtained from butyl titanate, the doping source and the fuel was from strontium nitrate and urea respectively. The samples were characterized by XRD, SEM, XPS, UV-Vis and FT-IR. The results showed that with the increase of doped Sr content from 0% to 1.0%, the average grain size of TiO_2 nanomaterials decreases from 21.3 to 19.2 nm, Sr was favorable for anatase formation and inhibited grain crystallization, and the sample has a larger specific surface area after doping. The degradation of organic wastewater containing methyl orange was carried out under UV irradiation for 20 min to discuss the effect of doping amount on the photocatalytic efficiency of the sample. The results indicated that the photocatalytic efficiency of doped Sr samples is higher than that of pure TiO_2, and the photocatalytic efficiency increases from 52.3% to 94.3% with the increase of Sr content. The maximum photocatalytic efficiency is the sample with a Sr content of 0.5%, and the maximum catalytic degradation rate is 95.6% after 20 min. It can be seen that the photon utilization rate of Sr-doped TiO_2 nanomaterials prepared rapidly by the microwave-induced combustion method has been significantly improved, and the mechanism of degradation of organic matter by nano Sr@TiO_2 was also studied and has the potential to be applied in the treatment of organic wastewater.

Keywords: Microwave induced combustion; Doping; Strontium; Titania; Photocatalysis; Wastewater treatment

1. Introduction

Due to their unique properties and structures, nanomaterials have been widely used in environmental protection, pollution treatment, biomedicine and other fields [1–7]. With the development of industrial society, water pollution has become increasing seriously. Therefore, nanomaterials have received more and more attention due to their excellent performance in treating water pollutants [8–12]. Under ultraviolet light irradiation, the anatase-type nano-TiO_2 material has excellent property in degrading organics in wastewater with high photocatalytic activity and good stability. Therefore, it has attracted more and more researchers' attention and has become the most promising photocatalysts for degradation of organics in wastewater [13]. However, anatase TiO_2 is only excited under ultraviolet light, and the photogenerated electrons and holes will recombine rapidly, which greatly reduces the photocatalytic efficiency of TiO_2 [14]. In order to overcome the above shortcomings, many researchers [15–25] have doped TiO_2 with metal or non-metal ions to prepare TiO_2 composite materials to suppress the recombination reaction

* Corresponding author.

† These authors contributed equally to this work.

of photogenerated electrons and holes, and broaden the wavelength absorption range of TiO_2 nanomaterials by improving the charge separation efficiency and narrowing the forbidden band gap respectively. The combination of n-type TiO_2 and p-type semiconductor to construct a p-n heterostructure is an effective way to improve the photoelectric conversion efficiency of TiO_2 [26]. Strontium titanate ($SrTiO_3$) is a p-type semiconductor with a perovskite structure. Its forbidden band gap is about 3.2 eV. Because of its high dielectric constant and large optical coefficient, it is widely used in capacitors, energy converters, optical device and memory device response [27]. Because the edge of the conduction band of $SrTiO_3$ is more negative than that of TiO_2 cathode [28], it is possible to improve the photoelectrochemical performance of $SrTiO_3$ composite TiO_2. Yang et al. [29], Ng et al. [30] found that $SrTiO_3/TiO_2$ photocatalysts can improve the charge separation efficiency and obtain higher photocatalytic activity. Zhang et al. [31] prepared the TiO_2-$SrTiO_3$ composite heterostructure by hydrothermal method and confirmed that the photoelectrochemical performance of TiO_2 has been significantly improved.

At present, the preparation methods of TiO_2 composite materials mainly include sol-gel method, hydrothermal method, microemulsion method, solution combustion method and microwave-induced combustion method. The advantages and disadvantages of various methods for preparing TiO_2 composite materials are shown in Table 1 [32–43].

Microwave-induced combustion method is also called microwave-assisted synthesis or microwave-activated combustion synthesis, which is a kind of self-propagating high-temperature synthesis technology. In the microwave electric field, the orientation of the polar molecule changes with the microwave, generating vibration and mutual friction effects, so that the temperature of the sample rises to the ignition point uniformly and quickly, and the combustion reaction proceeds smoothly, and the heat released can maintain the reaction smoothly. At the same time, it decomposes to produce a large amount of combustible gas. The whole reaction process lasts for a few minutes. The final combustion product is not easy to harden, fragile, and has a loose texture. In short, the microwave-induced combustion method has the advantages of simple operation, clean and efficient, low pollution, low energy consumption, no need for calcination, and small and uniform product particle size distribution [41–43].

In the field of TiO_2 composite material photocatalytic performance research, predecessors have done a lot of work: Kanakaraju et al. [44] prepared TiO_2/Mo photocatalysts with different molybdenum content by wet impregnation method, and systematically investigated the amount of photocatalyst, methyl orange Influencing factors such as initial concentration and initial pH, the optimal process conditions were determined. The optimal TiO_2/Mo (3 wt%) photocatalyst had a photodegradation efficiency of 94.5% for methyl orange within 120 min. Ao et al. [45] the sol-gel method to prepare TiO_2 nanomaterials, and obtained the highest methyl orange degradation rate of 49.28% after being degraded and irradiated under ultraviolet light for 4 h. Damdinova et al. [46] used the photoreduction method to deposit Ag_2MoO_4 nanoparticles on the surface of TiO_2 nanofibers, and degraded the methyl orange solution for 75 min under ultraviolet light irradiation, and the photocatalytic activity was 94.17%. In this paper, the microwave-induced combustion method was used to rapidly prepare nano-Sr@TiO_2 in 20 min, and the TiO_2 was modified to improve the utilization rate of light quantum. The result of catalytic degradation of methyl orange under ultraviolet light for 20 min showed that the degradation rate of 52.3% was compared with that of pure TiO_2, Sr@TiO_2 photodegradation rate has been improved, when the doped Sr amount is 0.5%, the highest catalytic efficiency is reached, which is 95.6%. And it is conducive to the practical application of

Table 1
Advantages and disadvantages of various methods for preparing TiO_2 nanocomposites [32–43]

Preparation methods	Advantages	Disadvantages
Sol–gel method [32–34]	Uniform sample particles	High cost, gas overflow can cause shrinkage and agglomeration easily during calcination process
Hydrothermal method [35,36]	Low energy consumption, controllable reaction atmosphere, low pollution, ideal crystal dispersion and crystallinity	Harsh Reaction conditions, difficult to observe the shape of the sample
Microemulsion method [37,38]	Mild reaction conditions	Surfactant is difficult to choose, the obtained particle crystal form is usually amorphous, and subsequent treatment is required
Solution combustion method [39,40]	Short preparation cycle, simple operation, and simple required equipment	Short and uncontrolled combustion process, the type and amount of fuel can easily affect the combustion process
Microwave induced combustion method [41–43]	Without calcination, small particle size and uniform distribution, clean and efficient, low pollution and energy consumption	Need to consider the influence of fuel type, microwave power, temperature, pH value and other factors to find suitable conditions

nano-TiO_2 materials and solves the serious water pollution problem.

2. Materials and methods

2.1. Materials

Butyl titanate (AR, 99%), isopropanol (AR, 99%), strontium nitrate (AR, 99%), nitric acid (GR, 99.8%), Chengdu Kelon Chemical Reagent Factory; Urea (AR, 99%), Chongqing Chuandong Chemical Group Co., Ltd.; Methyl Orange (AR, 99%), Chongqing Kelong Chemical Reagent Factory; Deionized water was used throughout the experiment.

2.2. Preparation of Sr@TiO_2

All chemicals applied in this work were used as received without further purification. The synthesis steps of Sr@TiO_2 samples are as follows: strontium nitrate (0.0000, 0.0016, 0.0022, 0.0027, 0.0055 respectively to control the Sr content of the sample) with 0.2839 g urea, 1 mL butyl titanate, 1 mL nitric acid(37%) and 4.5 mL of isopropanol were dissolved in 10 mL of distilled water in a crucible under magnetic stirring, and heated it until it becomes viscous. Then microwave the obtaining gunk for a few minutes. After heating, the samples of molar ratio of Sr to Ti of 0%, 0.3%, 0.4%, 0.5% and 1.0% were obtained (Table 2).

2.3. Characterization techniques

X-ray diffractometer (XRD, PANalytical X'Pert Powder, Netherlands), scanning electron microscope (SEM, Japan, JSM-7800F), X-ray spectrometer (XPS, Shimadzu, LabX XRD-6000), Ultraviolet-visible-near infrared spectrophotometer (UV-Vis, UV-3600), Fourier infrared spectrometer (FT-IR, USA, Nicolet5DX) to characterize the prepared samples.

2.4. Measurement of photocatalytic capacity

30 mg of the prepared Sr@TiO_2 sample and 200 mL of 20 mg/L methyl orange solution was added in a UV photocatalytic reactor, and stir for 30 min in the dark to achieve adsorption-desorption equilibrium. After the adsorption and desorption equilibrium, turn on the mercury UV lamp (250 W) approximately 20 cm above the UV photocatalytic reactor, and stir under the UV lamp for 20 min. Then the solution was centrifuged to obtain the supernatant, and the ultraviolet-visible spectrophotometer was used to measure the absorbance at 464 nm (the maximum absorption wavelength of methyl orange) to calculate the degradation rate. The percentage of degradation rate can be calculated as:

$$\eta = \frac{(A_0 - A_t)}{A_0} \times 100\% \quad (1)$$

where A_0 is the initial absorbance of methyl orange, and A_t is the absorbance after light time t.

Table 2
Dosage of reagent

n_{Sr}/n_{Ti} (%)	Dosage of urea	Dosage of strontium nitrate
0	0.2839	0.0000
0.3	0.2839	0.0016
0.4	0.2839	0.0022
0.5	0.2839	0.0027
1.0	0.2839	0.0055

3. Results and discussions

3.1. X-ray diffraction

Fig. 1 is the XRD pattern of TiO_2 doped with different amounts of Sr after microwave reaction for a few minutes. Among them, 2θ = 25.24°, 38.24°, 48.16°, 55.2° and 62.8° are the characteristic peaks of the anatase phase, and 2θ = 27.1° is the diffraction characteristic peak of the rutile phase. The average grain size and rutile content of the samples were calculated by Scherrer formula and Quantitative formula [47] respectively. According to the XRD patterns of anatase and rutile diffraction intensity, the Quantitative formula was used to calculate rutile content:

$$X = \frac{1}{(1 + 0.8 I_A / I_R)} \quad (2)$$

where I_A and I_R are the diffraction intensities of the diffraction plane of anatase (2θ = 25.4°) and rutile (2θ = 27.4°) respectively. The calculation results are listed in Table 3. As shown in Table 3, the rutile content of the sample decreased after doping with Sr, indicating that doping with Sr can inhibit the formation of TiO_2 rutile phase. It is well known that titanium dioxide has four different crystal structures, among which anatase photocatalytic performance is the best but unstable, rutile phase photocatalytic performance is second and the most stable, so anatase phase transformed into rutile phase easily. According to the research of Rodriguez-Talavera et al. [48], the radius of doped metal ions will

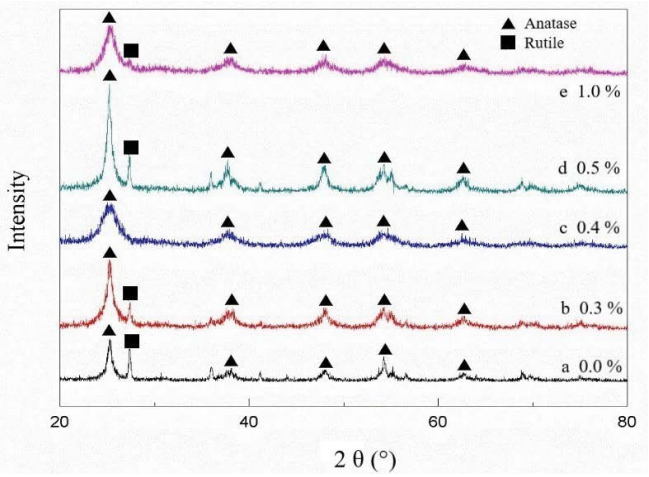

Fig. 1. XRD patterns of titanium dioxide samples with different strontium content: (a) 0%, (b) 0.3%, (c) 0.4%, (d) 0.5%, and (e) 1.0%.

Table 3
Effect of the Sr content on the rutile/anatase content and average grain size

Sr content (%)	0	0.3	0.4	0.5	1.0
Rutile content (%)	0.54	0.3	0	0.32	0.31
Average grain size (nm)	21.3	15.2	9.4	15.9	19.2

cause lattice distortion, and the stress field formed by such distortion will strongly hinder the movement of grain boundaries, thus preventing phase transformation.

At the same time, the average grain size decreased after Sr doping. Combined with the XRD pattern, it can be seen that the half-height width of the sample after Sr doping is larger than that of the undoped TiO_2, indicating that the doped ions have entered the TiO_2 crystal lattice and caused for a certain degree of lattice defects, the energy barrier of mutual diffusion between crystal grains is strengthened, and the growth of seed crystals is hindered to a certain extent, which makes the crystal average grain size smaller. In addition, the diffraction peak of SrO was not found in the spectrum, which may be due to the fact that Sr is amorphous or isomorphous substituted in TiO_2.

3.2. Fourier-infrared X-ray spectroscopy

Fig. 2 shows the infrared contrast spectra of TiO_2 and pure TiO_2 doped with 0.5% Sr. As can be seen from the figure, pure TiO_2 has a weak absorption in the mid-infrared region, while TiO_2 doped with Sr has a blue shift at the wavelength of 600–700 cm^{-1}. The peak within this wavelength range can be attributed to the stretching vibration of Ti–O–Ti bond in anatase. Since the atomic weight of Sr ion is larger than that of titanium atom, its stretching vibration frequency decreases after isomorphic substitution. The small peak around 1,100 cm^{-1} may be caused by the asymmetric vibration absorption of hydroxyl groups coordinated by some titanium ions. The absorption peak at 1,600 cm^{-1} should be caused by the bending vibration of the Ti–OH association peak. The peak around 3,100 cm^{-1} is the blue shift of the hydroxyl vibration absorption peak adsorbed on water molecules, which is caused by the enhanced polarity of TiO_2 surface due to the doping of Sr. The absorption peak at 1,400 cm^{-1} is a hybrid peak caused by insufficient purity of potassium bromide used in tablet pressing. Compared with pure TiO_2 infrared spectrogram, the Sr@TiO_2 samples is not a new peak, no residual organic matter in the preparation of sample, but in contrast is still in the peak shape and peak position slightly different aspects and so on, should be the introduction of the doping ion interaction force between the individual groups changes, thus make the key of the relative conditions change, affect the infrared spectrogram.

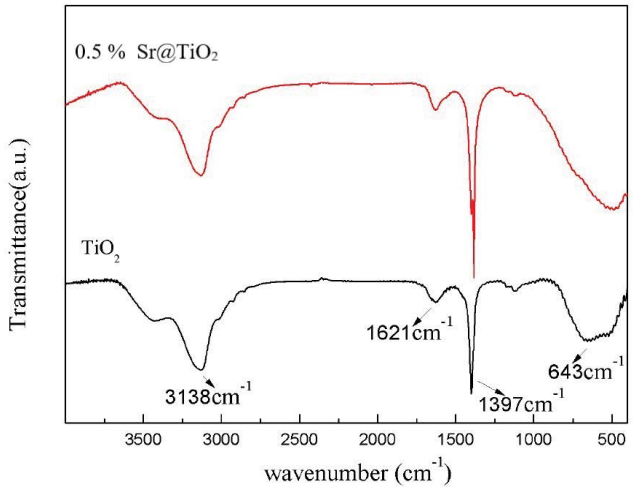

Fig. 2. FT-IR spectra of pure TiO_2 and 0.5% Sr@TiO_2.

3.3. Scanning electron microscopy

Fig. 3a shows the scanning electron microscopy of pure TiO_2, and Fig. 3b shows the scanning electron microscopy of TiO_2 with 0.5% Sr content. As can be seen from the figure, pure TiO_2 presents a loose block with a large volume, while TiO_2 doped with Sr presents an irregular sheet with an uneven size. In the process of sample preparation, the short time and high temperature of microwave heating could be caused an explosive and uneven combustion, this may be the cause of this situation.

3.4. X-ray photon spectroscopy

Fig. 4 shows the TiO_2 XPS spectrum with 0.5% Sr content after microwave reaction for 10 min. Fig. 4a confirms the existence of Ti, O, C and Sr. As can be seen from Fig. 4b, two peaks at 461.7 eV and 469.3 eV are observed in the Ti 2P spectrum, corresponding to 2p3/2 and 2p1/2 of Ti^{4+} respectively. Compared with pure TiO_2, the peak of O 1s moves towards the direction of high binding energy, and the peak of O 1s moves towards the direction of low binding energy, indicating that doping Sr enters the lattice. The lattice distortion of TiO_2 is caused, and more oxygen vacancies are generated, and the active reaction center of TiO_2 is increased. Fig. 4c is an XPS image of O 1s, with a peak value of 257.3 eV corresponding to O atoms bonded to metals (Ti and Sr) and a peak value of 529 eV corresponding to surface hydroxyl oxygen groups (O-H). Fig. 4d shows the XPS of Sr 3D, where two peaks at 133.7 and 135.4 eV can be observed respectively, which are Sr 3d5/2 and Sr 3d3/2. The lower energy peak is consistent with the perovskite structure $SrTiO_3$, while the higher energy peak can be attributed to the SrO complex.

3.5. Photocatalytic capacity

In general, photocatalysts generate e^- – h^+ pairs by absorbing photon energy, which can produce active substances such as O_2^-, OH for different photocatalysts, the number and types of active species produced are different under different conditions. The photocatalytic degradation process mainly consists of four steps: (1) absorbing light to generate e^- – h^+ pairs; (2) separation of excited charge; (3) transfer electrons and holes to the surface of the photocatalyst to avoid the recombination of electrons and holes; (4) generation of active species and degradation response of active species to target organic pollutants [49–51].

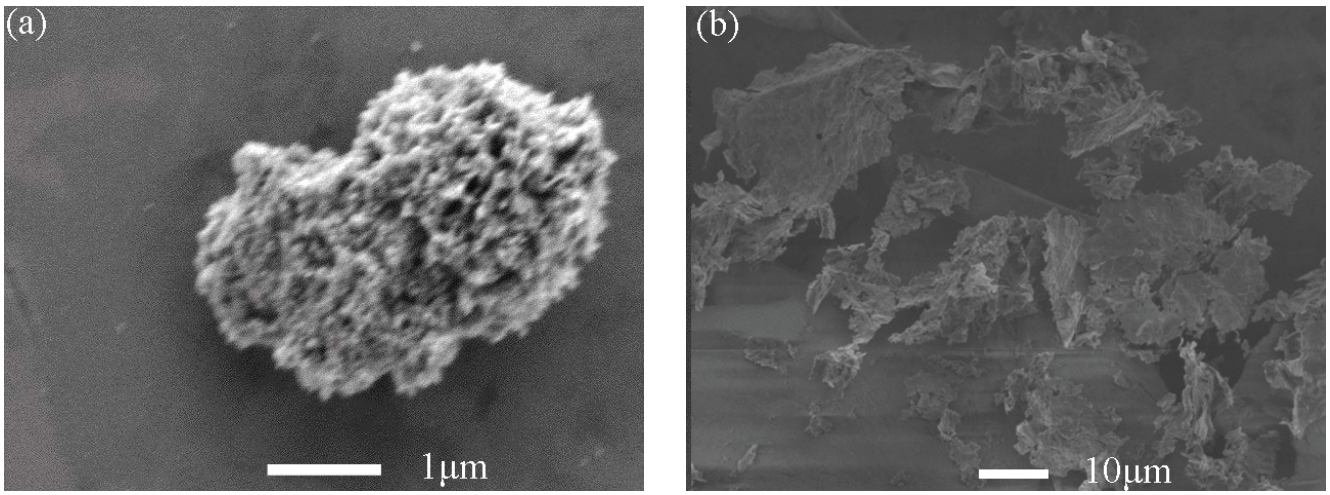

Fig. 3. SEM images of samples (a) pure TiO_2 and (b) 0.5% Sr@TiO_2.

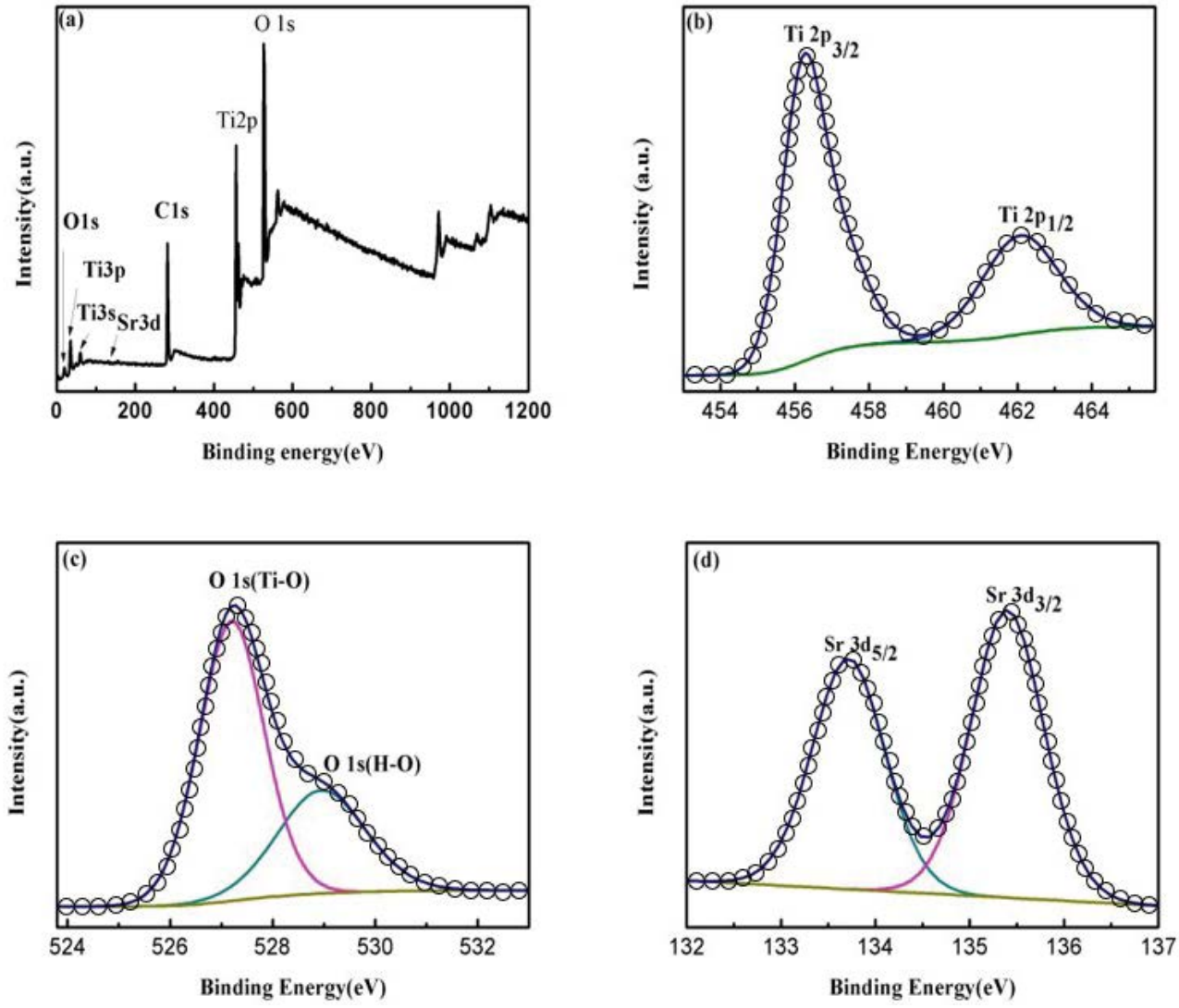

Fig. 4. XPS spectra of 0.5% Sr@TiO_2: (a) fully scanned spectra, (b) Ti 2p, (c) O 1s, and (d) Sr 3d.

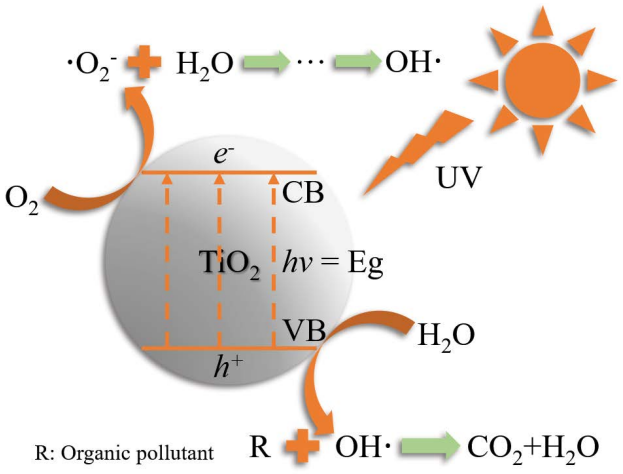

Fig. 5. Schematic diagram of TiO_2 photocatalytic reaction.

The mechanism of photocatalytic degradation of organic matter by TiO_2 nanomaterials is shown in Fig. 5 [52]. When the radiation energy (hv) is greater than or equal to the band gap energy (Eg), an electron from valence band (VB) is excited to transition to conduction band (CB), so that a valence band electron (e^-) is formed on CB and a valence band hole (h^+) is formed on VB [Eq. (3)]. And then, H_2O reacts with h^+ to form the highly oxidizing hydroxyl radical (OH) [Eq. (4)]. At the same time, a series of reactions [Eqs. (5)–(10)] between the e^- and O_2 adsorbed on the surface of titanium dioxide also produce hydroxyl radicals. With strong oxidation, OH can participate in the bond breaking reaction process of organic pollutant (*R*) and degrade them into harmless CO_2, H_2O and inorganic acids [53]. It's worth noting that the energy (hυ) of modified TiO_2 required for the electronic transition is significantly reduced, so the photo quantum utilization rate of Sr-doped TiO_2 nanomaterials prepared by microwave-induced combustion method is significantly improved.

$$TiO_2 + h\upsilon \rightarrow e^- + h^+ \quad (3)$$

$$H_2O + h^+ \rightarrow OH + H^+ \quad (4)$$

$$OH^- + h^+ \rightarrow OH \quad (5)$$

$$O_2 + e^- \rightarrow O_2^- \quad (6)$$

$$O_2^- + H_2O \rightarrow OOH + OH^- \quad (7)$$

$$2OOH \rightarrow O_2 + H_2O_2 \quad (8)$$

$$OOH + H_2O + e^- \rightarrow H_2O_2 + OH^- \quad (9)$$

$$H_2O_2 + e^- \rightarrow OH + OH^- \quad (10)$$

Fig. 6A shows UV-visible diffuse reflectance spectra of pure TiO_2 and Sr@TiO_2 samples. As can be seen from the figure, the absorption of Sr@TiO_2 sample mainly exists in the ultraviolet region, and the absorbance of the sample with the content of Sr at 0.5% is the highest. In addition, the sample also has partial absorption in the visible light region, which may be due to the fact that the rutile phase is mixed in the sample and Sr^{2+} enters the TiO_2 lattice at the same time, which changes the structure and results in absorption in the visible light region (400–500 nm). According to the band gap energy estimation formula Eg = 1,240/λg (λg/nm is the intersection of the vertical part and the horizontal part of the spectrum), the band gap width of pure TiO_2 is 2.91 eV, and the band gap widths of the samples with the Sr content of 0.3%, 0.4%, 0.5% and 1.0% are 2.86, 2.82, 2.81, and 2.86 eV, respectively. The band gap of Sr doped TiO_2 was lower than that of pure TiO_2, which expanded the visible light absorption range.

Fig. 6B shows the histogram of catalytic degradation of methyl orange by TiO_2 doped with different amounts of Sr for 20 min under UV light. It can be seen from the figure that the degradation rate of pure TiO_2 is 52.3%, while the photodegradation rate of TiO_2 doped with Sr is improved to some extent. The sample with Sr content of 0.5% has the highest catalytic efficiency of 95.6%, which corresponds to the maximum absorbance of the sample with Sr content of 0.5% in Fig. 6A. At the same time, it can be seen that with the increase of doping amount, the photocatalytic efficiency gradually increases. When it reaches 0.5%, the photocatalytic efficiency decreases again, but it is still higher than that of pure TiO_2. The main reasons are as follows: (1) There is more rutile in pure TiO_2, accounting for 0.54%, and the photocatalytic activity of rutile phase is low, which leads to the low photocatalytic activity of pure TiO_2. After doping with Sr, the content of rutile phase in the sample decreases, and a small amount of rutile phase in anatase is helpful for the separation of photogenerated electron-hole pairs, thus improving the photocatalytic efficiency. (2) Sr doping into TiO_2 causes lattice defects, inhibits grain growth, reduces the average grain size of doped samples, and increases the number of active photocatalytic centers, thus improving the catalytic efficiency. (3) In the low concentration range, the doping of Sr is beneficial to the separation of photoelectron–hole pairs, but when the doping concentration is too high, the composite center of photoelectron–hole pairs will be formed, thus reducing the photocatalytic efficiency.

The previous researches have done a lot of on the catalyst performance of the structures photocatalysis, such as [54–56]: Zahra Salehi et al. synthesized $Dy_2Ce_2O_7$ nanostructures by the facile salt-assisted combustion method, the maximum methyl orange dye degradation was about 80%; Zinatloo-Ajabshir et al. have been successfully synthesized pure praseodymium cerate ($Pr_2Ce_2O_7$) nanostructures via an improved Pechini procedure, the maximum methyl orange decomposition was about 92.1% under 50 min illumination of ultraviolet light; Morassaei et al. have prepared highly photocatalytically active $Nd_2Sn_2O_7$–SnO_2 nanocomposites through a simple salt-assisted combustion approach, the maximum methyl orange degradation was about 91% after 60 min illumination of UV light. The comparison between the samples prepared in this paper and them is shown in Table 4. It can be clearly seen from Table 4 that compared with other methods, the advantage of this paper is that the synthesis of Sr doped titanium dioxide nanomaterial by microwave induced

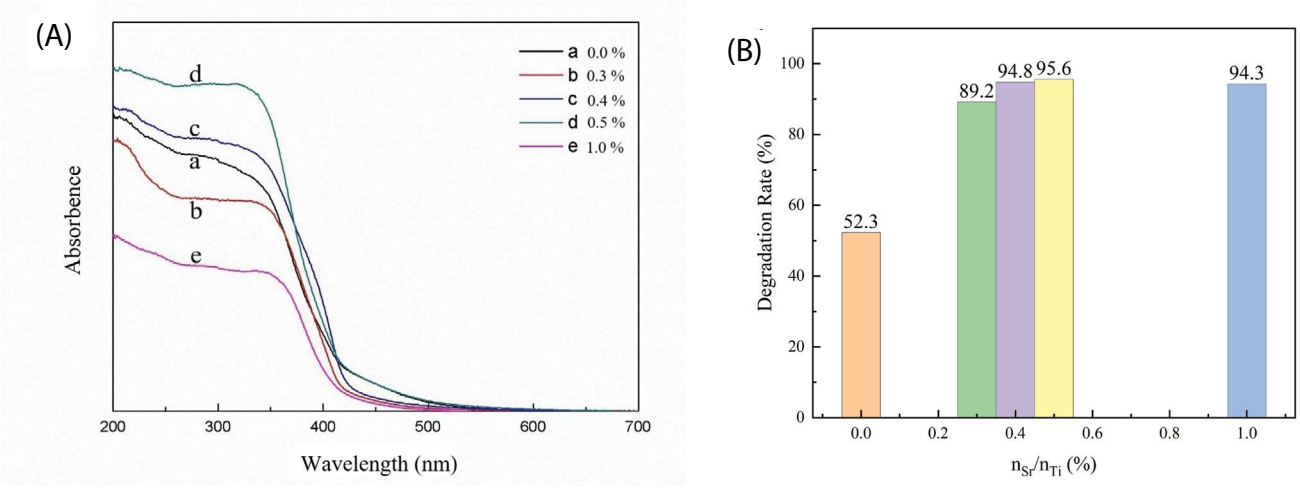

Fig. 6. (A) UV-Vis spectra of Sr@TiO_2 catalyst with different Sr loadings: (a) TiO_2, (b) 0.3%, (c) 0.4%, (d) 0.5%, (e) 1.0% and (B) histogram of photocatalytic degradation of methyl orange for samples doped with different amounts of Sr after 20 min.

Table 4
Comparison of the Sr@TiO_2 with other researchers' synthetic samples [54–56]

Samples	Method	Calcination time	Maximum degradation efficiency
$Dy_2Ce_2O_7$	Facile salt-assisted combustion method	4 h	80%
$Pr_2Ce_2O_7$	Improved Pechini procedure	5 h	92.1%
$Nd_2Sn_2O_7$–SnO_2	Salt-assisted combustion approach	4 h	91%
Sr@TiO_2	Microwave induced combustion method	Less than 20 min	95.6%

combustion method for the first time and the high photocatalytic degradation efficiency of methyl orange, up to 95.6%. In addition, the combustion time is less than 20 min and the sample synthesis time is greatly shortened correspondingly. At the same time, the equipment required for sample synthesis is very simple.

4. Conclusions

- TiO_2 nanomaterials doped with Sr were prepared by microwave induced combustion method rapidly. The preparation method is environmentally friendly, pollution-free, fast and efficient, and the preparation process is generally less than 20 min.
- The addition of Sr inhibits the transformation of anatase to rutile phase, and the morphology of the samples is more uniform and the average grain size is smaller.
- After the degradation of methyl orange solution by ultraviolet light for 20 min, it was found that the photocatalytic activity of the samples doped with Sr was greatly improved, and the photocatalytic rate was higher than that of pure TiO_2. With the increase of the doping amount of Sr, the photocatalytic efficiency first increased and then decreased, and the photocatalytic effect of the sample doped with 0.5% was the best, which was 95.6%. Therefore, the photo quantum utilization rate of Sr-doped TiO_2 nanomaterials prepared by microwave-induced combustion method is significantly improved, which is expected to be used to solve the pollution problem of organic matter in water.

References

[1] S.M. Hosseinpour-Mashkani, F. Mohandes, M. Salavati-Niasari, K. Venkateswara Rao, Microwave-assisted synthesis and photovoltaic measurements of $CuInS_2$ nanoparticles prepared by using metal–organic precursors, Mater. Res. Bull., 47 (2012) 3148–3159.
[2] A. Salehabadi, M. Salavati-Niasari, M. Ghiyasiyan-Arani, Self-assembly of hydrogen storage materials based multi-walled carbon nanotubes (MWCNTs) and $Dy_3Fe_5O_{12}$ (DFO) nanoparticles, J. Alloys Compd., 745 (2018) 789–797.
[3] S. Ahmadian-Fard-Fini, D. Ghanbari, M. Salavati-Niasari, Photoluminescence carbon dot as a sensor for detecting of Pseudomonas aeruginosa bacteria: hydrothermal synthesis of magnetic hollow $NiFe_2O_4$-carbon dots nanocomposite material, Composites, Part B, 161 (2019) 564–577.
[4] S. Zinatloo-Ajabshir, M.S. Morassaei, M. Salavati-Niasari, Eco-friendly synthesis of $Nd_2Sn_2O_7$-based nanostructure materials using grape juice as green fuel as photocatalyst for the degradation of erythrosine, Composites, Part B, 167 (2019) 643–653.
[5] S. Ahmadian-Fard-Fini, M. Salavati-Niasari, D. Ghanbari, Hydrothermal green synthesis of magnetic Fe_3O_4-carbon dots by lemon and grape fruit extracts and as a photoluminescence sensor for detecting of *E. coli* bacteria, Spectrochim. Acta, Part A, 203 (2018) 481–493.
[6] M. Ghanbari, M. Salavati-Niasari, Tl_4CdI_6 nanostructures: facile sonochemical synthesis and photocatalytic activity for removal of organic dyes, Inorg. Chem., 57 (2018) 11443–11455.

[7] M. Salavati-Niasari, Nanodimensional microreactor-encapsulation of 18-membered decaaza macrocycle copper(II) complexes, Chem. Lett., 34 (2005) 244–245.
[8] X.L. Liu, R. Ma, L. Zhuang, B.W. Hu, J.R. Chen, X.Y. Liu, X.K. Wang, Recent developments of doped g-C_3N_4 photocatalysts for the degradation of organic pollutants, Crit. Rev. Env. Sci. Technol., 51 (2021) 751–790.
[9] L. Yao, H. Yang, Z.S. Chen, M.Q. Qiu, B.W. Hu, X.X. Wang, Bismuth oxychloride-based materials for the removal of organic pollutants in wastewater, Chemosphere, 273 (2021) 128576, doi: 10.1016/j.chemosphere.2020.128576.
[10] M.J. Hao, M.Q. Qiu, H. Yang, B.W. Hu, X.X. Wang, Recent advances on preparation and environmental applications of MOF-derived carbons in catalysis, Sci. Total Environ., 760 (2021) 143333, doi: 10.1016/j.scitotenv.2020.143333.
[11] S.J. Yu, H.W. Pang, S.Y. Huang, H. Tang, S.Q. Wang, M.Q. Qiu, Z.S. Chen, H. Yang, G. Song, D. Fu, B.W. Hu, X.X. Wang, Recent advances in metal-organic framework membranes for water treatment: A review, Sci. Total Environ., 800 (2021).
[12] Q. Li, Z.S. Chen, H.H. Wang, H. Yang, T. Wen, S.Q. Wang, B.W. Hu, X.K. Wang, Removal of organic compounds by nanoscale zero-valent iron and its composites, Sci. Total Environ., 792 (2021) 148546, doi: 10.1016/j.scitotenv.2021.148546.
[13] M. Hojamberdiev, R.M. Prasad, K. Morita, Y. Zhu, M.A. Schiavon, A. Gurlo, R. Riedel, Template-free synthesis of polymer-derived mesoporous SiOC/TiO_2 and SiOC/N-doped TiO_2 ceramic composites for application in the removal of organic dyes from contaminated water, Appl. Catal., B, 115–116 (2012) 303–313.
[14] S. Peiris, H.B. de Silva, K.N. Ranasinghe, S.V. Bandara, I.R. Perera, Recent development and future prospects of TiO_2 photocatalysis, J. Chin. Chem. Soc., 68 (2021) 738–769.
[15] S. Mathew, P. Ganguly, S. Rhatigan, V. Kumaravel, C. Byrne, S.J. Hinder, J. Bartlett, M. Nolan, S.C. Pillai, Cu-doped TiO_2: visible light assisted photocatalytic antimicrobial activity, Appl. Sci. Basel, 8 (2018) 2067, doi: 10.3390/app8112067.
[16] X.D. Zhang, D. Yue, L. Zhang, S.W. Lin, Three-dimensional flexible Au nanoparticles-decorated TiO_2 nanotube arrays for photoelectrochemical biosensing, J. Mater. Sci. Technol., 56 (2020) 162–169.
[17] Y. Liu, Z.Z. Xiao, S. Cao, J.H. Li, L.Y. Piao, Controllable synthesis of Au-TiO_2 nanodumbbell photocatalysts with spatial redox region, Chin. J. Catal., 41 (2020) 219–226.
[18] S.J. Ki, Y.K. Park, J.S. Kim, W.J. Lee, H. Lee, S.C. Jung, Facile preparation of tungsten oxide doped TiO_2 photocatalysts using liquid phase plasma process for enhanced degradation of diethyl phthalate, Chem. Eng. J., 377 (2019) 120087, doi: 10.1016/j.cej.2018.10.024.
[19] Z.R. Yang, Z.Y. He, W.L. Wu, Y. Zhou, Preparation of graphene-TiO_2 photocatalysis materials by laser-induced hydrothermal method, Colloid Interface Sci. Commun., 42 (2021) 100408, doi: 10.1016/j.colcom.2021.100408.
[20] M. Zhao, F. Ling, Z. Gong, D. Zhuang, Absorption property in visible region of $TiO_{2-x}N_x$ films prepared by reactive sputtering, Chin. J. Mater. Res., 18 (2004) 108–112.
[21] Y. Liu, J. Li, X. Qiu, C. Burda, Novel TiO_2 nanocatalysts for wastewater purification: tapping energy from the sun, Water Sci. Technol., 54 (2006) 47–54.
[22] H. Wang, J.P. Lewis, Second-generation photocatalytic materials: anion-doped TiO_2, J. Phys.: Condens. Matter, 18 (2006) 421–434.
[23] D. Robert, Photosensitization of TiO_2 by MxOy and MxSy nanoparticles for heterogeneous photocatalysis applications, Catal. Today, 122 (2007) 20–26.
[24] Y. Yalcin, M. Kilic, Z. Cinar, Fe^{3+}-doped TiO_2: a combined experimental and computational approach to the evaluation of visible light activity, Appl. Catal., B, 99 (2010) 469–477.
[25] K.E. Karakitsou, X.E. Verykios, Effects of altervalent cation doping of TiO_2 on its performance as a photocatalyst for water cleavage, J. Phys. Chem., 97 (1993) 1184–1189.
[26] J.J. Lin, J.X. Shen, R.J. Wang, J.J. Cui, W.J. Zhou, P.G. Hu, D.O. Liu, H. Liu, J.Y. Wang, R.I. Boughton, Y.Z. Yue, Nano-p-n junctions on surface-coarsened TiO_2 nanobelts with enhanced photocatalytic activity, J. Mater. Chem., 21 (2011) 5106–5113.
[27] Y. Li, X.P. Gao, G.R. Li, G.L. Pan, T.Y. Yan, H.Y. Zhu, Titanate nanofiber reactivity: fabrication of $MTiO_3$ (M = Ca, Sr, and Ba) perovskite oxides, J. Phys. Chem. C, 113 (2009) 4386–4394.
[28] H.R. Zhang, G.S. Miao, X.P. Ma, B. Wang, Fabrication and photocatalytic property of one-dimensional $SrTiO_3/TiO_{2-x}N_x$ nanostructures, Int. J. Photoenergy, 2013 (2013), doi: 10.1155/2013/413507.
[29] Y. Yang, K. Lee, Y. Kado, P. Schmuki, Nb-doping of $TiO_2/SrTiO_3$ nanotubular heterostructures for enhanced photocatalytic water splitting, Electrochem. Commun., 17 (2012) 56–59.
[30] J. Ng, S.P. Xu, X.W. Zhang, H.Y. Yang, D.D. Sun, Hybridized nanowires and cubes: a novel architecture of a heterojunctioned $TiO_2/SrTiO_3$ thin film for efficient water splitting, Adv. Funct. Mater., 20 (2010) 4287–4294.
[31] J. Zhang, J.H. Bang, C.C. Tang, P.V. Kamat, Tailored TiO_2-$SrTiO_3$ heterostructure nanotube arrays for improved photoelectrochemical performance, ACS Nano, 4 (2010) 387–395.
[32] N. Uekawa, J. Kajiwara, K. Kakegawa, Y. Sasaki, Low temperature synthesis and characterization of porous anatase TiO_2 nanoparticles, J. Colloid Interface Sci., 250 (2002) 285–290.
[33] Y. Li, T.J. White, S.H. Lim, Low-temperature synthesis and microstructural control of titania nano-particles, J. Solid State Chem., 177 (2004) 1372–1381.
[34] L. Znaidi, R. Seraphimova, J.F. Bocquet, C. Colbeau-Justin, C. Pommier, A semi-continuous process for the synthesis of nanosize TiO_2 powders and their use as photocatalysts, Mater. Res. Bull., 36 (2001) 811–825.
[35] J. Yang, S. Mei, J.M.F. Ferreira, Hydrothermal synthesis of nanosized titania powders: influence of tetraalkyl ammonium hydroxides on particle characteristics, J. Am. Ceram. Soc., 84 (2001) 1696–1702.
[36] S.Y. Chae, M.K. Park, S.K. Lee, T.Y. Kim, S.K. Kim, W.I. Lee, Preparation of size-controlled TiO_2 nanoparticles and derivation of optically transparent photocatalytic films, Chem. Mater., 15 (2003) 3326–3331.
[37] M. Boutonnet, J. Kizling, P. Stenius, The preparation of monodisperse colloidal metal particles from micro-emulsions, Colloids Surf., 5 (1982) 209–225.
[38] S.S. Hong, M.S. Lee, S.S. Park, G.D. Lee, Synthesis of nanosized TiO_2/SiO_2 particles in the microemulsion and their photocatalytic activity on the decomposition of p-nitrophenol, Catal. Today, 87 (2003) 99–105.
[39] K.C. Patil, S.T. Aruna, T. Mimani, Combustion synthesis: an update, Curr. Opin. Solid State Mater. Sci., 6 (2002) 507–512.
[40] S.T. Aruna, M. Muthuraman, K.C. Patil, Synthesis and properties of Ni-YSZ cermet: anode material for solid oxide fuel cells, Solid State Ionics, 111 (1998) 45–51.
[41] Y.P. Fu, S. Tsao, C.T. Hu, Preparation of $Y_3Al_5O_{12}$: Cr powders by microwave-induced combustion process and their luminescent properties, J. Alloys Compd., 395 (2005) 227–230.
[42] Y.P. Fu, C.H. Lin, Fe/Sr ratio effect on magnetic properties of strontium ferrite powders synthesized microwave-induced combustion process, J. Alloys Compd., 386 (2005) 222–227.
[43] D.R. Baghurst, A.M. Chippindale, D.M.P. Mingos, Microwave syntheses for superconducting ceramics, Nature, 332 (1988) 311–311.
[44] D. Kanakaraju, M.A.A. Jasni, Y.C. Lim, A highly photoresponsive and efficient molybdenum-modified titanium dioxide photocatalyst for the degradation of methyl orange, Int. J. Environ. Sci. Technol., (2021) (in Press).
[45] A.O. Araoyinbo, M.M.A.B. Abdullah, A. Rahmat, A.I. Azmi, P. Vizureanu, W.M.F. Wan Abd Rahim, Preparation of heat treated titanium dioxide (TiO_2) nanoparticles for water purification, IOP Conf. Ser.: Mater. Sci. Eng., 374 (2018) 012084.
[46] S. Damdinova, W.C. Liu, S. Wang, B. Dugarov, Z.M. Su, Z.Q. Cheng, Preparation of coral-like Ag_2MoO_4-TiO_2 heterostructure and its photocatalytic properties, Mater. Chem. Phys., 235 (2019) 121765, doi: 10.1016/j.matchemphys.2019.121765.
[47] R.A. Spurr, H. Myers, Quantitative analysis of anatase-rutile mixtures with an x-ray diffractometer, Anal. Chem., 29 (1957) 760–762.
[48] R. RodriguezTalavera, S. Vargas, R. Arroyo Murillo, R. Montiel Campos, E. Haro Poniatowski, Modification of the phase

transition temperatures in titania doped with various cations, J. Mater. Res., 12 (1997) 439–443.
[49] M.Q. Qiu, B.W. Hu, Z.S. Chen, H. Yang, L. Zhuang, X.K. Wang, Challenges of organic pollutant photocatalysis by biochar-based catalysts, Biochar, 3 (2021) 117–123.
[50] Y.L. Zhu, W.Z. Wang, J. Ni, B.W. Hu, Cultivation of granules containing anaerobic decolorization and aerobic degradation cultures for the complete mineralization of azo dyes in wastewater, Chemosphere, 246 (2020) 125753, doi: 10.1016/j.chemosphere.2019.125753.
[51] M. Fang, X.L. Tan, Z.X. Liu, B.W. Hu, X.K. Wang, Recent progress on metal-enhanced photocatalysis: a review on the mechanism, Research, 2021 (2021).
[52] M.S. Dieckmann, K.A. Gray, A comparison of the degradation of 4-nitrophenol via direct and sensitized photocatalysis in TiO_2 slurries, Water Res., 30 (1996) 1169–1183.
[53] L.Z. Sun, J.R. Bolton, Determination of the quantum yield for the photochemical generation of hydroxyl radicals in TiO_2 suspensions, J. Phys. Chem., 100 (1996) 4127–4134.
[54] Z. Salehi, S. Zinatloo-Ajabshir, M. Salavati-Niasari, Novel synthesis of $Dy_2Ce_2O_7$ nanostructures via a facile combustion route, RSC Adv., 6 (2016) 26895–26901.
[55] S. Zinatloo-Ajabshir, Z. Salehi, M. Salavati-Niasari, Preparation, characterization and photocatalytic properties of $Pr_2Ce_2O_7$ nanostructures via a facile procedure, RSC Adv., 6 (2016) 107785–107792.
[56] M.S. Morassaei, S. Zinatloo-Ajabshir, M. Salavati-Niasari, Simple salt-assisted combustion synthesis of $Nd_2Sn_2O_7$-SnO_2 nanocomposites with different amino acids as fuel: an efficient photocatalyst for the degradation of methyl orange dye, J. Mater. Sci. - Mater. Electron., 27 (2016) 11698–11706.